Available online at www.sciencedirect.com
SCIENCE DIRECT
Journal of Catalysis 242 (2006) 131–141
JOURNAL OF CATALYSIS
www.elsevier.com/locate/jcat

Effects of ozone pretreatment on the performance of Au/TiO_2 catalyst for CO oxidation reaction

K.Y. Ho [a,b], K.L. Yeung [b,*]

[a] *Environmental Engineering Program, The Hong Kong University of Science and Technology, Clear Water Bay, Kowloon, Hong Kong*
[b] *Department of Chemical Engineering, The Hong Kong University of Science and Technology, Clear Water Bay, Kowloon, Hong Kong*

Received 9 April 2006; revised 5 June 2006; accepted 5 June 2006

Available online 7 July 2006

Abstract

O_3-pretreated O_3-Au/TiO_2 catalyst exhibited better catalyst dispersion and stability compared with O_2-pretreated O_2-Au/TiO_2. Ozone effectively removed the carbonaceous byproducts of catalyst preparation that oxygen was unable to completely decompose. This resulted in the poor catalyst dispersion and a bimodal gold particle size distribution of O_2-Au/TiO_2. The catalyst performance was tested for the CO oxidation reaction and compared with the gold reference catalyst (GRC). The reaction was carried out in an in situ DRIFTS apparatus that provides real-time monitoring of surface reaction and simultaneous collection of reaction conversion data. Both Au/TiO_2 catalysts displayed higher conversion rates for CO oxidation reaction compared with GRC. Gold sintering was evident for the O_2-Au/TiO_2 and GRC after the CO oxidation reaction at 473 K, and both catalysts suffered a loss in activity. The formation of oxidic gold observed in O_3-Au/TiO_2 is expected to afford a stronger metal–support interaction and may be the reason for the excellent stability of this catalyst against sintering.

Keywords: Gold; Titanium dioxide; Carbon monoxide; Ozone; In situ spectroscopy; DRIFTS

1. Introduction

TiO_2-supported gold catalysts (Au/TiO_2) are excellent catalysts for the CO oxidation reaction and can catalyze the reaction even at 200 K [1]. The ability of Au/TiO_2 to oxidize CO at low temperatures has applications in air pollution control [2–5] and in fuel and gas processing [6,7]. The catalytic activity of the gold catalyst depends on the size of the gold particles [8,9] and the phase structure of the TiO_2 support [10], and is sensitive to the catalyst preparation and pretreatment conditions [11–15]. The pretreatment of catalyst in oxidizing and reducing conditions is an established method for preparing highly dispersed, supported metal catalysts [16–20]. The deposited catalyst precursors are decomposed during oxidation and reduced to active metals during the reduction process. However, this procedure is not normally used in gold catalyst preparation, because of the difficulty in oxidizing gold.

The work of Valden et al. [8] showed that gold with a size of 3.5 nm performed best for the CO oxidation reaction at 350 K. The Au/TiO_2 prepared by deposition–precipitation followed by calcination at 673 K showed that gold with a size of 3 nm performed best for the CO oxidation reaction at room temperature [9]. Air calcination could strengthen the interaction between gold and the TiO_2 support. This was demonstrated by Haruta et al. [21] using a mechanical mixture of colloidal gold and TiO_2 powder. These authors claimed that a stronger metal–support interaction is responsible for the improved catalyst activity at higher calcination temperatures. Calcination also rids the surface of carbonaceous contaminant from the support or precursor materials [22]. It has been shown that subambient CO oxidation reactions are catalyzed by the low-coordinated sites on the gold surface and along the perimeter of gold and the TiO_2 support. The best catalyst, according to Boccuzzi and Haruta [1,23,24], was obtained by calcinations at 573 K. Calcination at temperatures above 573 K runs a high risk of particle sintering, because gold nanoparticles are known to melt at temperature as low as 600 K [25]. This work compares the catalytic performance of Au/TiO_2 catalysts pretreated in air and an

* Corresponding author. Fax: +852 23580054.
E-mail address: kekyeung@ust.hk (K.L. Yeung).

0021-9517/$ – see front matter
doi:10.1016/j.jcat.2006.06.005

ozone–oxygen mixture at a mild temperature of 473 K. The CO oxidation reaction was monitored by a diffuse reflectance infrared Fourier transform spectroscopy (DRIFTS) and gas chromatography to provide information on the surface reaction and catalyst reactivity. The in situ DRIFTS was carried out at different reaction temperatures.

2. Experimental

2.1. Preparation of Au/TiO_2 catalysts

Three gold catalysts were investigated in this work. A gold reference catalyst (Au/TiO_2, GRC type A) was purchased from the World Gold Council. The GRC-A catalyst contained 1.47 wt% gold loading and a reported average gold diameter of 3.7 nm. This catalyst was used without additional pretreatment. Two batches of gold catalysts were prepared on nanostructured TiO_2 support. The nanostructured TiO_2 was prepared using a modified sol–gel process [26]. This new synthesis procedure allowed direct control of the particle and aggregate sizes, crystallinity [27,28], and surface properties [29,30] of the nanostructured TiO_2. The synthesis was carried out in a dry nitrogen glovebox at room temperature. The titanium isopropoxide (TIP, 98%, Acros Organics) precursor was added with rapid mixing to a water–isopropanol (IPA, 99.7%, BDH) solution to give a final molar composition of 1 TIP:24 IPA:5 H_2O. Amorphous titanium oxide gel spheres of uniform size and shape were formed during the rapid hydrolysis of the titanium organometal precursor. The reaction mixture was aged for an hour, before the powder was recovered by filtration. The TiO_2 nanocrystals were crystallized from the amorphous gel spheres by thermal treatment at 723 K for 3 h in a high-temperature furnace (Carbolite BOF 11/13). A free-flowing TiO_2 powder was obtained and used as support for the gold catalyst.

The gold was deposited on the nanostructured TiO_2 support at a neutral pH from a gold chloride solution. First, 1 g of the TiO_2 powder was dispersed in double-distilled, deionized water, and then 20 mL of 2.5 mM hydrogen tetrachloroaurate(III) trihydrate solution was added. The mixture was aged at room temperature for 30 min in a dark, sealed container. The catalyst was recovered by filtration and washed with hot water (i.e., 368 K), before drying in a vacuum oven at 298 K for 24 h. The catalyst powder was divided into two batches for pretreatment in dry air (22% O_2 and 78% N_2) and ozone (100 ppm O_3/O_2) at 473 K for 5 h. The ozone was generated from high-purity oxygen gas (99.97%) by an electrical discharge ozone generator (Trailigaz, Ozoconcept OZC100), and the ozone feed concentration was monitored by a gas analyzer (Trailigaz, Uvozon TLG 200). The O_2-Au/TiO_2 and O_3-Au/TiO_2 samples were characterized and tested for the CO oxidation reaction.

2.2. Characterization of Au/TiO_2 catalysts

The physiochemical properties of the nanostructured TiO_2 support and gold catalysts were characterized by different techniques. Thermogravimetric and differential thermal analyses (TGA/DTA; Setaram) were carried out for both the amorphous and nanostructured TiO_2 samples. Monitoring the weight loss and heat flow during the programmed heating (i.e., 298 to 1073 K at 5 K/min) of the sample in air provides important information on the crystallization of TiO_2 nanoparticles during the thermal treatment. The nanostructured TiO_2 was examined by X-ray diffraction (XRD; Philips PW1830) and micro-Raman spectroscopy (Renishaw) to determine its phase structure, crystallinity, and particle size. The XRD data for the TiO_2 powder were obtained for $20^\circ < 2\theta < 65^\circ$ at a scan rate of 0.05° using a Cu$K\alpha$ X-ray source with a graphite monochromator. The TiO_2 powder was coated onto a glass slide and analyzed by Renishaw RM series Raman microscope using a 20-mW Argon laser (514.5 nm). The signals between 50 and 1000 cm^{-1} were collected at a resolution of 1.5 cm^{-1}. The textural properties of the TiO_2, including the specific surface area, pore structure, and pore volume, were determined by nitrogen physisorption (Coulter SA 3100). The sample was outgassed in vacuum at 393 K for 2 h before the analysis. The surface elemental compositions of the TiO_2 support were analyzed by X-ray photoelectron spectroscopy (XPS; Physical Electronics PHI 5600).

The gold contents of the O_2-Au/TiO_2, O_3-Au/TiO_2, and GRC-A catalysts were measured by dissolving a sample of the catalysts in aqua regia and analyzing with inductively coupled plasma atomic emission spectroscopy (ICP-AES; Perkin–Elmer Optima 3000XL) after dilution. XPS analysis provided information on surface elemental compositions of the gold catalysts. The XPS used a monochromatic aluminum X-ray source at a shallow grazing angle, giving a sampling depth of <1 nm. The size and shape of the gold catalyst particles were imaged by high-resolution transmission electron microscopy (HRTEM; JEOL JEM 2010). The particle size distribution was obtained by measuring more than 100 individual gold particles, and the average particle size was calculated by

$$\bar{d} = \frac{\sum n_i d_i}{\sum n_i}, \tag{1}$$

where n_i is the number of particles with a diameter d_i. XRD and nitrogen physisorption were carried out to monitor changes in the physical and textural properties of the catalysts after pretreatment and reaction.

2.3. CO oxidation reaction on Au/TiO_2 catalysts

The catalytic oxidation of carbon monoxide on the gold catalysts was carried out in the operando DRIFTS setup shown in Fig. 1. The setup consists of a gas delivery system, a diffuse reflectance IR reactor cell from Harrick (Fig. 1a), a Perkin–Elmer FTIR (GX 2000), and a Hewlett Packard gas chromatograph (HP 6890). The carbon monoxide (99.9%) and dry, synthetic air (22% O_2 and 78% N_2) were metered by an electronic mass flow controller (Sierra 810S-Series Mass-Trak) and mixed before entering the reactor cell. The catalyst powder was placed in a heated receptacle inside the diffuse reflectance infrared reactor cell. The reactor temperature was monitored by a K-type thermocouple and heated with a cartridge heater. Circulating cooling water in the outer reactor shell helped maintain the reactor temperature. The gas flow was directed through the thin catalyst

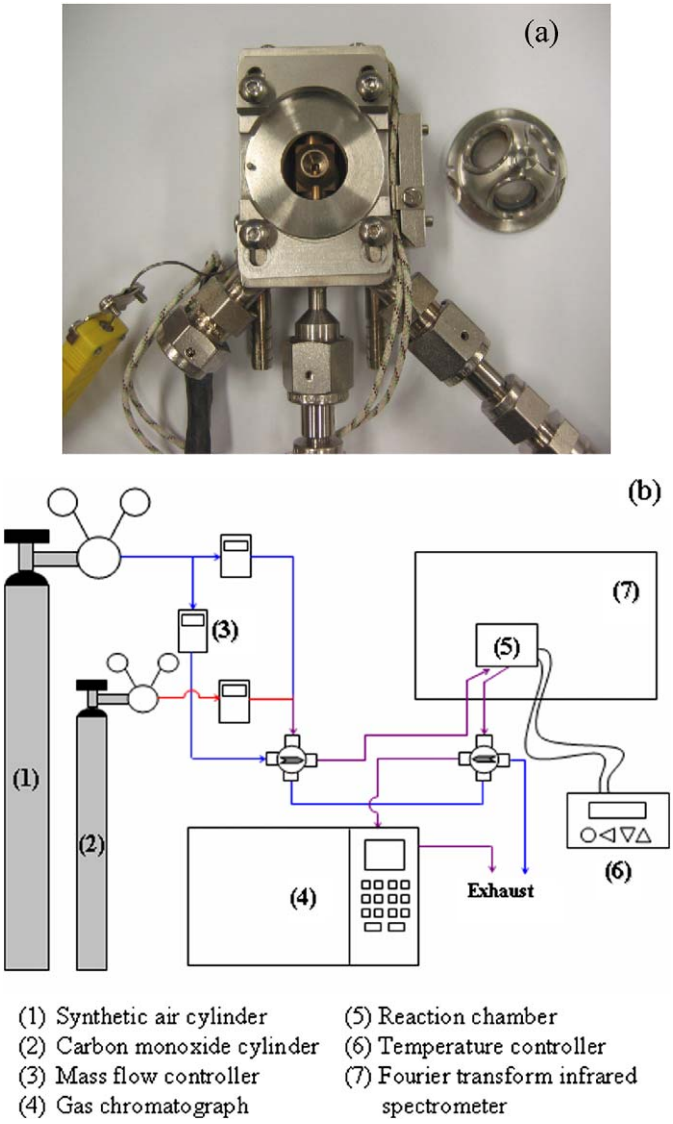

Fig. 1. (a) A picture of the diffuse reflectance reaction cell and (b) schematic diagram of the reactor setup.

bed and exited the reactor for analysis by an on-line gas chromatograph. The reaction mixture was separated by a CTR-1 column (Alltech, $6' \times 1/4''$ o.d.) and analyzed by a thermal conductivity detector. The reactor cell was placed in the Harrick diffuse reflection attachment unit. The praying mantis mirror arrangement directs the incident beam onto the surface of the catalyst bed and collects the diffusion reflectance for analysis by the FTIR spectrometer. The reactor cell was designed to minimize reflection losses from the windows and maximize the light interaction with the sample. A total of 64 scans at a resolution of 0.5 cm^{-1} were obtained from 500 to 4000 cm^{-1} with an optical path difference velocity of 2 $cm\,s^{-1}$.

Each reaction experiment was carried out using 30 mg of gold catalyst. The catalyst powder was placed in the sample holder of the diffuse reflectance cell and purged with dry synthetic air at room temperature to remove moisture and weakly adsorbed gases. The outgassing was monitored by DRIFTS, and the reaction was carried out only when the adsorbed contaminants were decreased to a background level. Carbon monoxide was mixed with synthetic air to give a reactant feed of 2.5% CO in air. The feed flow rate was maintained at 200 sccm (i.e., standard $cm^3\,min^{-1}$) to give a space velocity of 132,000 h^{-1}. The surface reaction was monitored with DRIFTS, and the exit gas was analyzed to determine the reaction conversion and selectivity. The CO oxidation reaction was carried out at different reaction temperatures and times.

3. Results and discussion

3.1. Au/TiO_2 catalysts

The nanostructured TiO_2 support was crystallized from the amorphous titania gel spheres prepared by the modified sol–gel method [26]. The TGA/DTA thermographs in Fig. 2a show that dehydration occurred at temperatures below 473 K and accounts for most of the weight loss, whereas the exothermic heat flow at 473–573 K corresponds to the decomposition and oxidation of the residual organic molecules from the solvent and unreacted alkoxide groups. The transformation from amorphous to crystalline anatase TiO_2 was marked by an exothermic heat flow at 673 K [27]. Therefore, it is sufficient to calcine the titania gel spheres at 732 K for 3 h to remove all of the organic residues (Fig. 2b) and to crystallize the anatase TiO_2 nanoparticles (Fig. 2c). The Raman spectrum of the sample displays all of the characteristic peaks of anatase TiO_2, including the signals at 636 and 142 cm^{-1}, assigned to the E_g mode; the signal at 516 cm^{-1}, assigned to the doublet of A_{1g} and B_{1g} modes; and the signal at 395 cm^{-1}, assigned to the B_{1g} mode [31]. The size of the TiO_2 nanoparticles was determined by XRD peak broadening to be 13 ± 0.5 nm and was confirmed by TEM. The textural property of the nanostructured TiO_2 support was analyzed by a nitrogen physisorption experiment. The support has a BET surface area of 70 ± 2 m^2/g and displays a type-II isotherm with a type-H4 hysteresis, as shown in Fig. 2d. The type-II isotherm is characteristic of multilayer adsorption on nonporous or macroporous solids, and the type-H4 hysteresis is often associated with slit-shape microporosity [32]. This is consistent with the structure of the nanostructured TiO_2 support. The amorphous titania gel spheres were transformed during calcination into aggregate clusters of 100 ± 6 nm anatase TiO_2 nanoparticles.

The Au/TiO_2 catalyst was prepared from $HAuCl_4$ solution at a neutral pH. According to Gavriilidis and co-workers [33,34] $[AuCl(OH)_3]^-$ is the main gold species at pH 7, with trace amounts of $[AuCl_2(OH)_2]^-$ and $[Au(OH)_4]^-$ anions. It had been suggested by Moreau et al. [15] that a neutral $Au(OH)_3 \cdot H_2O$ species could exist in equilibrium with the gold anions at pH $\geqslant 6$. The nanostructured TiO_2 support has an isoelectric point of 6.5 ± 0.5, meaning that the TiO_2 surface has a weak negative charge at pH 7. A decrease in pH from 7 to 5.5 ± 0.5 was observed during catalyst preparation. A possible scheme for deposition of gold onto the TiO_2 surface is illustrated in Scheme 1. The gold anions react with the hydroxyl groups on the TiO_2 surface, forming surface gold complexes. The HCl byproduct produced by the complexation reaction

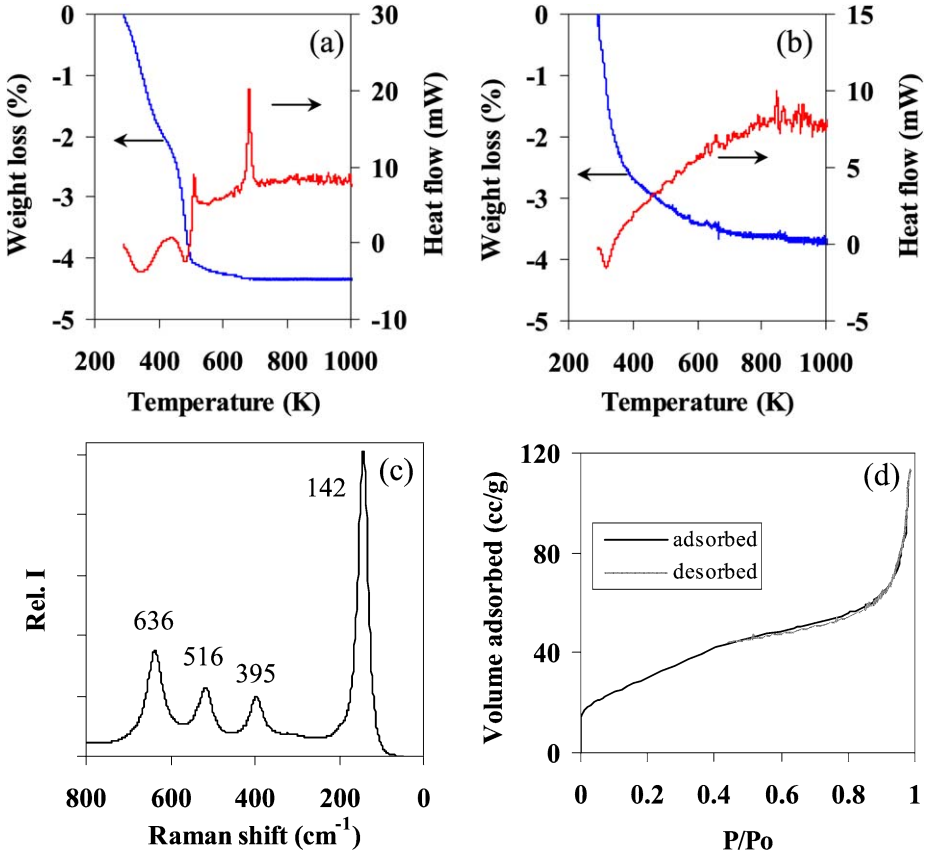

Fig. 2. Plots of the thermogravimetric and differential thermal analyses of (a) amorphous titania gel particles and (b) nanostructured TiO_2, (c) micro-Raman spectrum and (d) N_2 adsorption–desorption isotherm of nanostructured TiO_2.

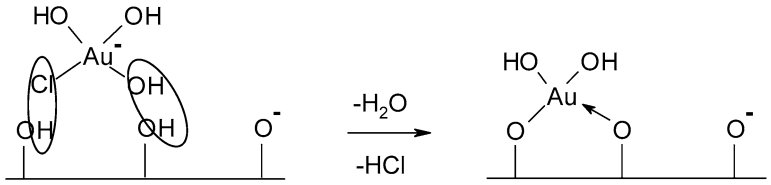

Scheme 1. Absorption of $[AuCl(OH)_3]^-$ on slightly negatively charged TiO_2 surface and possible subsequent reactions.

could explain the increased acidity observed during gold deposition. The Au/TiO_2 catalyst was analyzed by ICP-AES to have a gold content of 0.58 ± 0.20 wt%.

Catalyst pretreatment in oxidizing and reducing conditions is an established method for preparing highly dispersed supported metal catalysts. Oxidation helps decompose the catalyst precursor and disperse the catalyst on the support surface. However, there have not been many studies on the effects of oxidation on gold catalyst, because gold, being a noble metal, is difficult to oxidize. Indeed, gold catalyst remained metallic even after high-temperature (573 K) treatment in oxygen. O_2-Au/TiO_2 and O_3-Au/TiO_2 were prepared by oxidizing Au/TiO_2 in dry air (22% O_2 and 78% N_2) and a 100-ppm O_3–O_2 mixture, respectively. The pretreatment temperature was kept low at 473 K to avoid catalyst sintering. Ozone is a stronger oxidizer than the oxygen in air. Table 1 lists the standard electrode potentials for ozone, oxygen, and different gold species [35]. The XPS analysis of O_2-Au/TiO_2 shows the Au 4f peaks are located at 83.9 and 87.6 eV, indicating that the gold in the pretreated catalyst is in a reduced state (Fig. 3a) [36]. Fig. 3b shows that the ozone-treated gold catalyst, O_3-Au/TiO_2, has broader Au 4f peaks shifted toward higher energies, indicating the presence of oxidic gold [37]. A properly stored O_3-Au/TiO_2 catalyst treated by ozone will exhibit oxidic gold under XPS even after 1 month in storage. The third gold catalyst was the GRC purchased from

Table 1
Standard electrode potentials [27]

Reaction	E° (V)
$O_3 + 2H^+ + 2e^- \rightleftharpoons O_2 + H_2O$	2.076
$O_2 + 4H^+ + 4e^- \rightleftharpoons 2H_2O$	1.229
$Au(OH)_3 + 3H^+ + 3e^- \rightleftharpoons Au + 3H_2O$	1.45
$AuOH^{2+} + H^+ + 2e^- \rightleftharpoons Au^+ + H_2O$	1.32
$AuCl_4^- + 3e^- \rightleftharpoons Au + 4Cl^-$	1.002
$Au^{3+} + 3e^- \rightleftharpoons Au$	1.498
$Au^{3+} + 2e^- \rightleftharpoons Au^-$	1.401
$Au^{2+} + e^- \rightleftharpoons Au^+$	1.8
$Au^+ + e^- \rightleftharpoons Au$	1.692

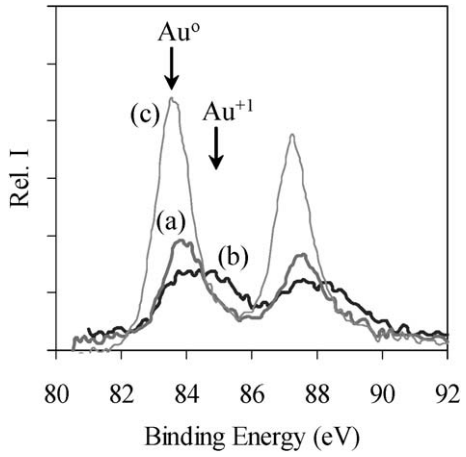

Fig. 3. XPS spectra of (a) O_2-Au/TiO_2, (b) O_3-Au/TiO_2, and (c) GRC-A.

the World Gold Council. The GRC contained 1.42 wt% gold loading according to ICP-AES and displayed Au^0 $4f_{7/2}$ and $4f_{5/2}$ peaks, as shown in Fig. 3c. The stronger XPS signal from the GRC sample is due to the higher gold content of this catalyst.

Fig. 4 displays the XRD patterns of nanostructured TiO_2 support, Degussa P25, and the three gold catalysts, O_2-Au/TiO_2, O_3-Au/TiO_2, and GRC. The nanostructured TiO_2 is pure anatase and displays only the characteristic diffraction peaks of anatase TiO_2, as shown in Fig. 4a. The XRD patterns of the gold catalysts prepared from this support (i.e., O_2-Au/TiO_2 and O_3-Au/TiO_2) are shown in Figs. 4b and 4c. No gold diffraction peaks are seen; the figure shows only the diffraction peaks belonging to the support. This can be explained by the low gold metal loadings and the small size of the gold particles. The XRD pattern of GRC (Fig. 4d) shows diffraction peaks belonging to anatase and rutile TiO_2, but not to gold. The diffraction pattern in Fig. 4d is very similar to that of commercial Degussa P25 titanium dioxide (Fig. 4e). The sizes of the anatase and rutile TiO_2 calculated from the diffraction peak broadening are 24 and 38 nm, respectively. The specific surface area of the Degussa P25 is 50 ± 4 m^2/g, less than that of the nanostructured TiO_2. The specific surface areas of the gold catalysts do not differ from the starting support material, as should be expected given the mild catalyst preparation and pretreatment conditions.

The TEM micrographs of the gold catalysts are displayed in Figs. 5a–5c. The TEM micrograph of the O_2-Au/TiO_2 in Fig. 5a shows a catalyst with gold nanoparticles uniformly dispersed on aggregate clusters of TiO_2 nanocrystals. This figure clearly shows that TiO_2 nanocrystals measuring 10–15 nm in diameter aggregate to form 100-nm globular clusters. The gold particle size distribution was obtained from measurements of more than 100 individual gold nanoparticles and is plotted in Fig. 6a. The catalyst displays a bimodal particle size distribution comprising two populations with average particle diameters of 1.5 ± 0.2 and 6 ± 0.6 nm, respectively. The mean gold particle size is 2.3 ± 0.2 nm. The ozone-treated gold catalyst, O_3-Au/TiO_2 shown in Fig. 5b, is similar in appearance to O_2-Au/TiO_2 but has a normal particle size distribution centered at 1.5 nm, as shown in Fig. 6b. The mean gold particle size is 2.4 ± 0.3 nm. A similar analysis of the GRC catalyst reveals a significantly different catalyst structure, as shown in Fig. 5c. The GRC's TiO_2 support is coarser and has an irregular shape. The GRC catalyst has a normal particle size distribution (Fig. 6c) and a mean gold particle size of 2.1 ± 0.1 nm. Table 2 summarizes the properties of the three gold catalysts.

3.2. CO oxidation reaction

The catalytic oxidation of carbon monoxide on gold catalysts was carried out in an in situ DRIFTS. The reactions were performed at 298, 323, 373, and 473 K in flowing reactant mixture containing 2.5% CO in dry air at a space velocity of 132,000 h^{-1}. The surface reaction was monitored by DRIFTS, and the composition of reaction gas mixture was analyzed by on-line gas chromatography to determine the reaction conversion and selectivity. Fig. 7 plots the results of the reaction study. Arrhenius plots of the CO conversion rates for the O_2-Au/TiO_2, O_3-Au/TiO_2, and GRC catalysts are shown in Fig. 7a. The O_2-Au/TiO_2 catalyst displays the highest CO conversion rate of the three gold catalysts investigated in this work. Room temperature CO conversion rates are 13.5 mmol s^{-1} g_{Au}^{-1} for this catalyst, 10.5 mmol s^{-1} g_{Au}^{-1} for O_3-Au/TiO_2, and 4.5 mmol s^{-1} g_{Au}^{-1} for GRC (Table 2). Fig. 7a shows that the GRC catalyst exhibits

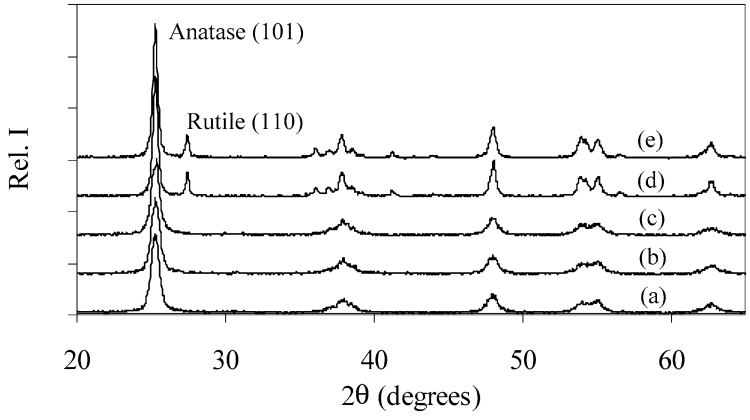

Fig. 4. X-ray diffraction patterns of (a) nanostructured TiO_2, (b) O_2-Au/TiO_2, (c) O_3-Au/TiO_2, (d) GRC-A, and (e) Degussa P25.

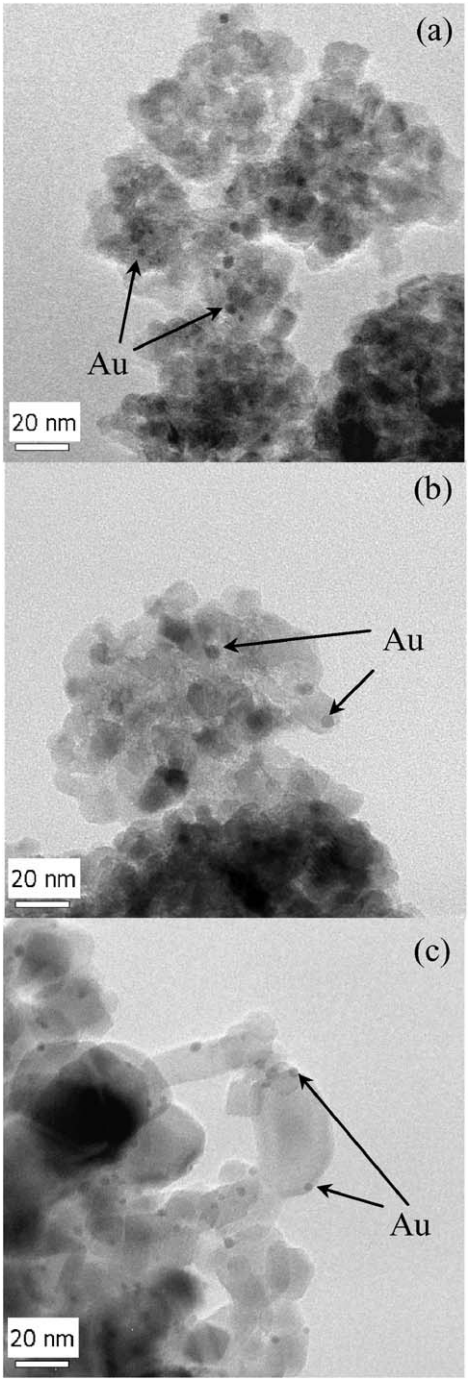

Fig. 5. HR-TEM pictures of fresh (a) O_2-Au/TiO_2, (b) O_3-Au/TiO_2, and (c) GRC-A catalyst.

a relatively greater dependence on the temperature compared with the two Au/TiO_2 catalysts. The activation energies, E_a, are 1.03 ± 0.29 kJ mol^{-1} for O_2-Au/TiO_2, 0 ± 0.57 kJ mol^{-1} for O_3-Au/TiO_2, and 2.02 ± 0.11 kJ mol^{-1} for GRC. The low activation energies were due to the high conversion values (>80%) obtained under the reaction conditions. Low mass transfer rate could also play a role, but the high feed flow rate makes this unlikely.

Fig. 7b plots the IR spectra collected by the in situ DRIFTS during CO oxidation on the O_2-Au/TiO_2 catalyst. The fresh catalyst before reaction (Fig. 7b (i)) displays IR signals from adsorbed water molecules at 1620 and 3200 cm^{-1}. The broad band centered at around 3200 cm^{-1} is believed to result from the superpositioning of υ_{OH} modes from water molecules coordinated to the Ti^{4+} cations and from interactions between surface hydroxyl groups [38,39]. Also present are infrared signals at 3690, 3665, and 3630 cm^{-1} attributed to the stretching of adsorbed water and vibrations of surface hydroxyl groups [40]. These signals are common to all three gold catalysts, as shown in Figs. 7c–7d. Fig. 7b (i) shows that O_2-Au/TiO_2 also contains trace amounts of carbonate (i.e., 1435 and 1350 cm^{-1}) from the Na_2CO_3 used in the catalyst preparation. The IR signals for adsorbed water disappear within minutes of introducing the reactant mixture at room temperature, as shown in Fig. 7b (ii). CO oxidation is an exothermic reaction, and the heat produced can desorb the water from the catalyst surface. A slight decrease in surface hydroxyl group can be observed from the signal at 3665 cm^{-1}. This signal diminishes with increasing reaction temperature (Fig. 7b, (iii) to (v)). This could be due to their outgassing at high temperature, but it is also possible that these hydroxyls participate in the reaction and are consumed accordingly.

CO adsorption on the catalyst produces two bands, one at 2173 cm^{-1}, corresponding to the stretching of CO coordinated to Ti^{4+} of the anatase support [41], and at the other at 2116 cm^{-1}, assigned to CO adsorbed on the gold surface [1]. Experiments showed that the signal at 2173 cm^{-1} is present only at high CO concentrations. This signal disappears when the CO level drops below 250 ppm, and only the 2116 cm^{-1} band is detected. The reaction produces carbon dioxide, and adsorbed CO_2 (i.e., 2346 cm^{-1}) is present on the catalyst. The DRIFTS spectra of adsorbed CO and CO_2 show no significant changes with increasing reaction temperature (Fig. 7b), because the CO reaction over the O_2-Au/TiO_2 catalyst is relatively insensitive to temperature (Fig. 7a). Surface carbonate species are present on the catalyst, as shown in Fig. 7b. Noncoordinated carbonate formed by adsorption of CO_2 product is the main species. It has a characteristic signal at 1430 cm^{-1} [8]. The noncoordinated carbonate peak diminishes with increasing reaction temperature and is replaced by the growing signals at 1550 and 1350 cm^{-1} assigned to monodentate carbonate species [22]. The presence of bidentate carbonate species can be safely excluded because of the absence of signature bands at 1620 and 1090 cm^{-1}. Surface carbonate species are formed on the TiO_2 support and may compete with oxygen adsorption. Haruta et al. [23] proposed that the CO reaction occurs at the perimeter interface between CO adsorbed on the Au surface and molecular oxygen adsorbed on the support surface with the formation of carbonate species.

CO reaction on the O_3-Au/TiO_2 catalyst behaves differently than the calcined gold catalyst, as shown in Fig. 7c. The ozone treatment at 473 K effectively removes the trace carbonate left on the gold catalyst during catalyst preparation (Fig. 7c (i)). The CO oxidation reaction at room temperature results in rapid surface dehydration, exposing the IR signal for surface hydroxyls at 3665 cm^{-1}. A small shoulder peak at 3700 cm^{-1} is also seen on the sample. Reactions at higher temperatures show a

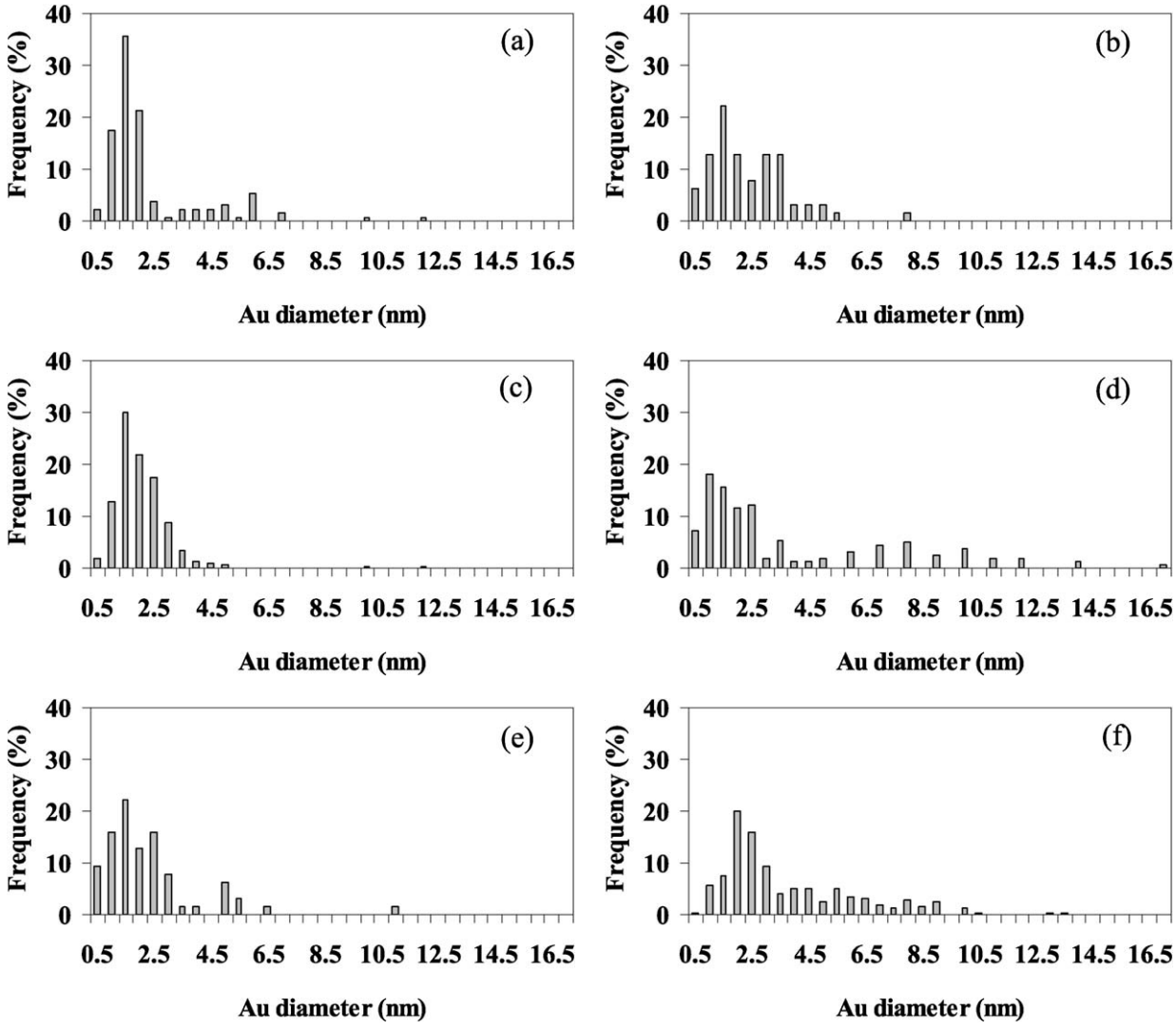

Fig. 6. Gold particle size distributions of fresh (a) O_2-Au/TiO_2, (b) O_3-Au/TiO_2, (c) GRC-A and spent (d) O_2-Au/TiO_2, (e) O_3-Au/TiO_2, and (f) GRC-A catalyst.

Table 2
Physicochemical properties of gold catalysts

Catalyst	Pretreatment	BET area (m^2/g)	TiO_2 crystal size[a] (nm)	Au loading[b] (wt%)	Au particle size[c] (nm)	R_0[d] (mmol s^{-1} g_{Au}^{-1})
O_2-Au/TiO_2	O_2, 473 K, 5 h	70 ± 2	12 (anatase)	0.58	2.32 ± 0.22	13.5
O_3-Au/TiO_2	100 ppm O_3/O_2, 473 K, 5 h	68 ± 2	13 (anatase)	0.59	2.41 ± 0.25	10.5
GRC[e]	None	50 ± 4	24 (anatase) 38 (rutile)	1.42	2.05 ± 0.08	4.5

[a] Calculated from XRD peak broadening of anatase TiO_2(101) and rutile TiO_2(110).
[b] Measured by ICP-AES after acid digestion.
[c] Mean particle size measured by TEM.
[d] Initial CO reaction rate for $[CO]_{Air} = 2.5\%$, $Q = 200$ sccm and 298 K.
[e] Gold reference catalyst from the World Gold Council.

decrease in the 3665 cm^{-1} signal and an increase in the peak at 3700 cm^{-1} corresponding to strongly bound isolated hydroxyl groups on the anatase surface [11]. Fig. 8a documents the first few minutes of introducing carbon monoxide to the catalyst. IR bands at 2128 and 2169 cm^{-1} appear immediately after the addition of carbon monoxide. The signal at 2169 cm^{-1} had been assigned to CO adsorption on oxidic gold sites by Baiker and co-workers [22] and the signal at 2128 cm^{-1} had been variously assigned to CO on Au^+ complex and on positively polarized gold interacting with surface superoxide species or adsorbed peroxidic oxygen molecules observed under low-temperature reactions (i.e., 85–90 K) [42]. The presence of oxidic gold species is consistent with the broader Au 4f peaks of this sample (Fig. 3b). The signal at 2169 cm^{-1} is gradually replaced by

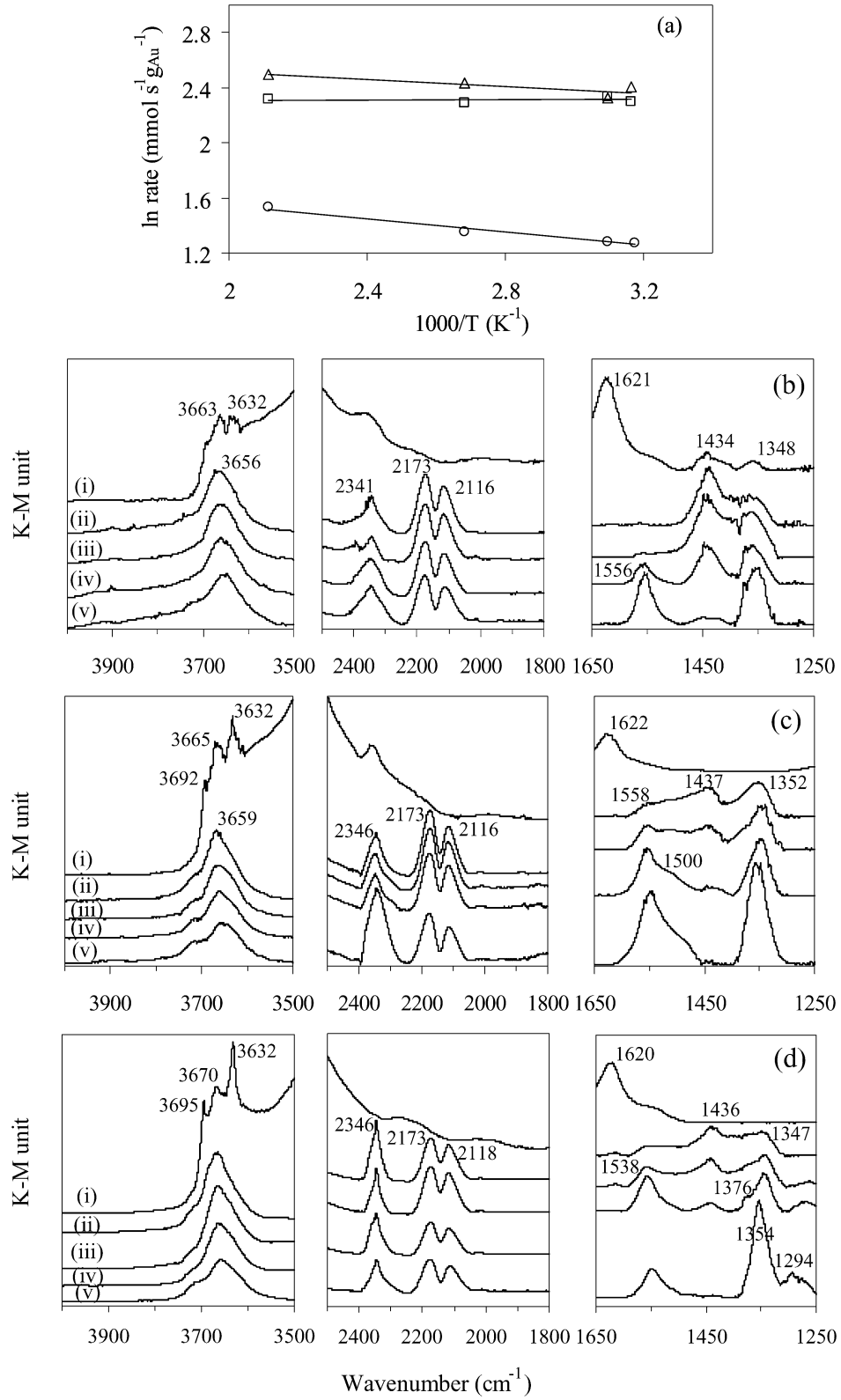

Fig. 7. (a) Arrhenius plot of O_2-Au/TiO_2 (△), O_3-Au/TiO_2 (□), and GRC-A (○) heated from 298 to 473 K. DRIFTS spectra of (b) O_2-Au/TiO_2, (c) O_3-Au/TiO_2, and (d) GRC-A—no reaction (i) and with reaction at 298 K (ii), 323 K (iii), 373 K (iv), and 473 K (v). ([CO] = 2.5%, [O_2] = 22%, balanced by N_2, space velocity = 132,000 h^{-1}.)

a new signal at 2176 cm^{-1} corresponding to CO-Ti^{4+} surface species, and the 2116 cm^{-1} peak appears with the formation of metallic gold under reducing CO atmosphere. The reduction process is evident from the large CO_2 peak at 2354 cm^{-1} appearing on the addition of carbon monoxide (Fig. 8a). This signal rapidly decreases with the formation of metallic gold and

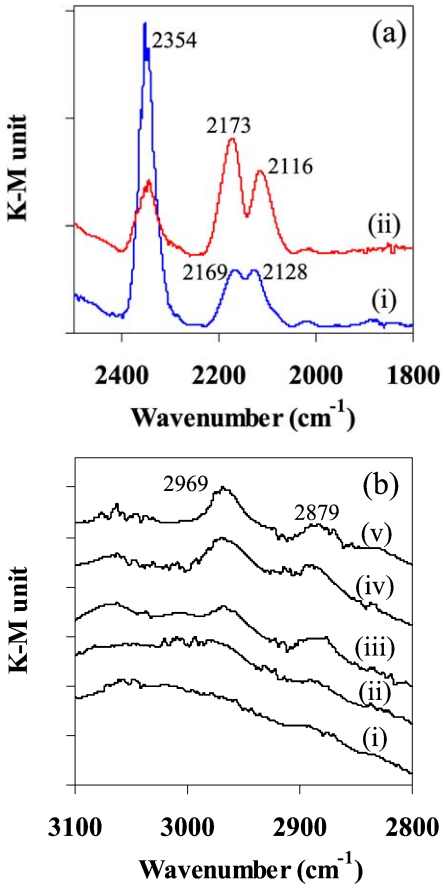

Fig. 8. DRIFTS spectra of 2.5% CO with synthetic air flow in 1 min (i) and 3 min (ii) at 298 K over O_3-Au/TiO_2. (b) DRIFTS spectra of O_3-Au/TiO_2 before reaction (i) and with 2.5% CO with synthetic air flow at 298 K (ii), 323 K (iii), 373 K (iv), and 473 K (v).

the inception of a normal CO reaction. Indeed, a shift in Au 4f to lower energies occurs observed after the reaction. However, careful analysis indicates the presence of trace oxidic gold in the predominantly reduced gold catalyst.

The O_2-Au/TiO_2 and O_3-Au/TiO_2 have comparable conversion, but the CO_2 peak signal for the latter catalyst is stronger. Also, monodentate carbonate (i.e., 1550 and 1350 cm^{-1}) formation occurs at a lower temperature for this catalyst. Both the adsorbed CO_2 and monodentate carbonate increase with higher temperatures, whereas the noncoordinated carbonate (i.e., 1430 cm^{-1}) displays a decreasing trend. The signal at 1500 cm^{-1} could be due to carboxylate species bound to a titanium atom [43]. There is no evidence of bidentate carbonate species on the catalyst. Fig. 8b shows the presence of additional IR bands at 2800–3100 cm^{-1} during reaction at higher temperatures. The peaks at 2969 cm^{-1} and 2879 cm^{-1} could arise from a combination of (COO) + δ (CH) and υ_s (CH) vibration modes of a bidentate formate [4,44]. The formation of formate species could be fueled by the reaction between adsorbed CO with a bridging hydroxyl groups. This may partially explain the decreased signal of the hydroxyl group (i.e., 3659 cm^{-1}) with reaction, as shown in Fig. 7c. It is important to note that the IR bands of monodentate carbonate at 1550 and 1350 cm^{-1} are also congruent with the IR band of formate species, that is, υ_{as} (COO) at 1575 cm^{-1}, υ_s (COO) at 1358 cm^{-1}, and δ (CH) at 1323 cm^{-1} [22,45].

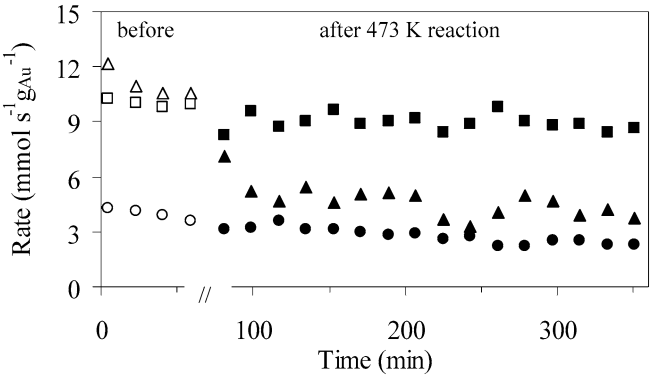

Fig. 9. CO conversion rate for room temperature CO oxidation reaction over O_2-Au/TiO_2 (△), O_3-Au/TiO_2 (□), and GRC-A (○) before (empty symbol) and after (filled symbol) reaction at 473 K.

Fig. 7d shows the surface reaction on the commercial GRC sample. This catalyst has a higher gold loading and was used without further pretreatment, as recommended. The GRC catalyst also undergoes rapid dehydration during the room temperature reaction. The IR band at 3665 cm^{-1} belonging to surface hydroxyl decreases with higher reaction temperature, whereas the 3700 cm^{-1} peak increases, as shown in the figure. Both CO peaks at 2116 (CO-Au) and 2173 (CO-Ti^{4+}) cm^{-1} are present, as is the CO_2 peak at 2346 cm^{-1}. The CO peaks are weaker than the other two catalysts, reflecting the higher CO conversion. The intensity of the CO peaks decreases as the CO conversion rate increases with increasing reaction temperature (Fig. 7d). Both noncoordinated and monodentate carbonates are present on the catalyst at room temperature reaction. The surface carbonate species increase with temperature up to 373 K. Two new peaks, at 1376 and 1294 cm^{-1}, are detected on the GRC sample during the CO oxidation reaction at 473 K. These two peaks may arise from the symmetric stretching of carboxylate and monodentate carbonate [46].

3.3. Catalyst stability

Fig. 9 plots CO conversion rate at room temperature for the three gold catalysts before and after reaction at 473 K. The initial reaction rates of the fresh catalysts are 13.5 mmol s^{-1} g_{Au}^{-1} for O_2-Au/TiO_2, 10.5 mmol s^{-1} g_{Au}^{-1} for O_3-Au/TiO_2, and 4.5 mmol s^{-1} g_{Au}^{-1} for GRC. The O_2-Au/TiO_2 catalyst shows decreasing rates after the high-temperature reaction. The gold catalysts display lower conversion rates after high-temperature reaction, as shown in the figure. The O_2-Au/TiO_2 catalyst loses roughly 50% of its initial activity, to give a conversion rate of 7.1 mmol s^{-1} g_{Au}^{-1}, whereas GRC activity decreases by about 33%. Only the O_3-Au/TiO_2 catalyst is able to maintain its initial reactivity. Catalyst deactivation has a strong correlation with gold particle size and a weak dependence on the surface carbonate species. Figs. 6d–6f plot the gold particle size distributions of the spent gold catalysts. The O_2-Au/TiO_2 catalyst shows a shift in the bimodal particle size distribution toward larger particles with a significant increase in the fraction of gold particles

with diameter >6 nm. Calculations shows that the average particle size of the gold catalyst increases from the original 2.3 nm to 3.6 nm after the reaction at 473 K. Similarly, the gold particle size distribution of GRC exhibits a marked increase in large particles, as shown in Fig. 6f. The average gold particle size increased from 2.1 to 3.7 nm. The rapid growth of gold particles in the GRC sample may be related to the stability of gold on rutile TiO_2. Kolmakov and Goodman [47] reported that the gold clusters on TiO_2(110) with diameter <4 nm are unstable toward sintering at around 450 K under oxygen pressure >1.3 kPa. It is clear that both the O_2-Au/TiO_2 and GRC catalysts suffer from sintering and loss of catalytic surface area resulting in a marked decrease in catalyst activity for CO oxidation. The deactivation is less evident for the GRC, because of the higher gold loading of this catalyst.

The gold particle size distribution of the ozone pretreated O_3-Au/TiO_2 catalyst remains unchanged before and after reaction at 473 K, and the catalyst activity remains stable. The average gold particle size is 2.4 nm for the fresh catalyst and 2.3 nm for spent catalyst. Ozone is a strong oxidizer (Table 1) that can effectively decompose the catalyst precursor and remove the byproducts of the catalyst preparation (e.g., carbonates and carbonaceous species) that oxygen cannot remove under the mild pretreatment temperature used in the study (cf. Figs. 7b and 7c). Ozone is strong enough to oxidize gold (Table 1), resulting in improved catalyst dispersion, as shown in Fig. 6b. Table 1 indicates that under mild temperature, oxygen is insufficient for oxidizing most of the common gold precursor species found in preparing gold catalysts. This could explain the poor catalyst dispersion and bimodal particle size distribution of the air-calcined O_2-Au/TiO_2 catalyst. The oxidic gold in O_3-Au/TiO_2 is expected to have a stronger interaction with the TiO_2 metal-oxide support, resulting in better catalyst stability. A strong metal–support interaction would prevent catalyst sintering and loss of activity. High-temperature air calcination is commonly used to strengthen the metal–support interaction in gold on titanium dioxide [17,21], but there is greater risk of metal sintering at these elevated temperatures [1].

The in situ DRIFTS spectra in Figs. 7b–7d show surface carbonates in all three catalysts, including GRC, that persist up to high temperatures. Konova et al. [41] suggested that formation of carbonate adlayer on the oxide support could cause catalyst deactivation. The adsorbed carbonates compete with oxygen for adsorption sites on the surface of TiO_2, decreasing the availability of active oxygen for the reaction. The experimental results suggest that gold sintering has greater effects on deactivation compared with the formation of surface carbonate. Fig. 9 shows that both GRC and O_2-Au/TiO_2 suffer further deactivation even during room temperature reaction. The GRC loses an additional third of its activity at the end of the reaction. The final conversion rate of 2.3 mmol s^{-1} g_{Au}^{-1} is less than half the original activity of the fresh catalyst. Fig. 9 shows the that conversion rate of O_2-Au/TiO_2 decreased from 7.1 to 3.8 mmol s^{-1} g_{Au}^{-1} after 4.5 h of reaction at room temperature. The final catalyst activity is less than 1/3 of the original value. The in situ DRIFTS technique provides real-time monitoring of the surface reaction; Fig. 10 plots the intensity of monodentate carbonate

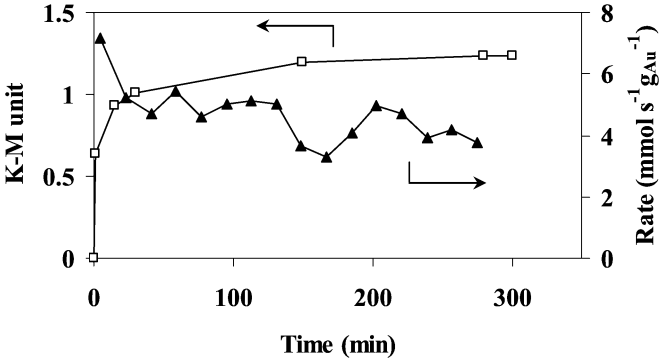

Fig. 10. Infrared intensity of monodentate carbonate and conversion rate for room temperature CO reaction over O_2-Au/TiO_2 catalyst after reaction at 473 K.

(1370 cm^{-1}) from the DRIFTS spectra for the room temperature reaction of O_2-Au/TiO_2 shown in Fig. 9. The accumulation of monodentate carbonate on the catalyst surface occurs during the deactivation of O_2-Au/TiO_2.

4. Conclusion

The pretreatment of gold catalyst with a stronger oxidizer, ozone, resulted in better catalyst dispersion and stability. The ozone pretreatment was conducted at a mild temperature (i.e., 473 K) to avoid the risk of catalyst sintering. Ozone effectively removed the carbonaceous byproducts of catalyst preparation that oxygen was unable to decompose completely at the mild pretreatment temperature. The O_2-pretreated gold catalyst, O_2-Au/TiO_2, had poor dispersion, as demonstrated by the bimodal gold particle size distribution, compared with the O_3-pretreated O_3-Au/TiO_2 catalyst. Both catalysts displayed higher conversion rates for the CO oxidation reaction compared with the commercial GRC supplied by the World Gold Council. The fresh catalysts had room temperature CO conversion rates of 13.5 mmol s^{-1} g_{Au}^{-1} for O_2-Au/TiO_2, 10.5 mmol s^{-1} g_{Au}^{-1} for O_3-Au/TiO_2, and 4.5 mmol s^{-1} g_{Au}^{-1} for GRC.

The gold catalysts were tested for CO oxidation reaction in an in situ DRIFTS apparatus that provides real-time monitoring of surface reaction and conversion. Catalyst dehydration was immediate, and adsorbed water was completely removed at the start of the room temperature CO oxidation reaction. The presence of oxidic gold and its rapid reduction during reaction was observed for O_3-Au/TiO_2. Surface carbonate species were present in all three catalysts. Noncoordinated and monodentate carbonates were observed, but bidentate carbonate was not found. The accumulation of surface carbonate species could affect catalyst reactivity and may be the source of catalyst deactivation. However, catalyst sintering remained the most important reason for catalyst deactivation. Gold sintering was evident for O_2-Au/TiO_2 and GRC, and both catalysts suffered a loss in activity. Both catalysts displayed a bimodal particle size distribution and larger gold particle sizes. Ozone pretreatment led to a more stable O_3-Au/TiO_2 catalyst. Both gold particle size and catalyst reactivity remained unchanged for this catalyst despite reaction at high temperatures.

Acknowledgments

Funding for this project was provided by the Innovation and Technology Commission of the Hong Kong SAR Government (ITS/176/01C), Veolia Environnement (Veolia Water Asia and Anjou Recherches), Honeywell HK, Chiaphua Industries Ltd., and Orkney Environmental Technology Ltd. K.Y. Ho acknowledges a postgraduate scholarship from the Environmental Engineering Program. The authors thank the Material Preparation and Characterization Facility (MCPF) of the Hong Kong University of Science and Technology for the use of their XRD, TEM, and TGA/DTA equipment for catalyst characterization.

References

[1] F. Boccuzzi, A. Chiorino, M. Manzoli, P. Lu, T. Akita, S. Ichikawa, M. Haruta, J. Catal. 202 (2001) 256.
[2] D. Andreeva, T. Tabakova, L. Ilievaa, A. Naydenov, D. Mehanjiev, M.V. Abrashev, Appl. Catal. A 209 (2001) 291.
[3] M. Daté, Y. Ichihashi, T. Yamashita, A. Chiorino, F. Boccuzzi, M. Hartua, Catal. Today 72 (2002) 89.
[4] T. Kecskés, J. Raskó, J. Kiss, Appl. Catal. A 273 (2004) 55.
[5] M.A. Centeno, M. Paulis, M. Montes, J.A. Odriozola, Appl. Catal. B 61 (2005) 177.
[6] D. Andreeva, Gold Bull. 35 (2002) 82.
[7] M. Manzoli, A. Chiorino, F. Boccuzzi, Appl. Catal. B 57 (2004) 201.
[8] M. Valden, X. Lai, D.W. Goodman, Science 281 (1998) 1647.
[9] M. Haruta, S. Tsubota, T. Kobayashi, H. Kageyama, M.J. Genet, B. Delmon, J. Catal. 144 (1993) 175.
[10] W. Yan, B. Chen, S.M. Mahurin, V. Schwartz, D.R. Mullins, A.R. Lupini, S.J. Pennycook, S. Dai, S.H. Overbury, J. Phys. Chem. B 109 (2005) 10676.
[11] M.A. Bollinger, M.A. Vannice, Appl. Catal. B 8 (1996) 417.
[12] G.R. Bamwenda, S. Tsubota, T. Nakamura, M. Haruta, Catal. Lett. 44 (1997) 83.
[13] R. Zanella, S. Giorgio, C.R. Henry, C. Louis, J. Phys. Chem. B 106 (2002) 7634.
[14] R. Zanella, S. Giorgio, C.H. Shin, C.R. Henry, C. Louis, J. Catal. 222 (2004) 357.
[15] F. Moreau, G.C. Bond, A.O. Taylor, J. Catal. 231 (2005) 105.
[16] J.R. Anderson, M. Boudart, Catalysis: Science and Technology, Springer-Verlag, Berlin, 1984, pp. 247–248.
[17] G. Ertl, H. Knzinger, J. Weitkamp (Eds.), Preparation of Solid Catalysts, Wiley–VCH, Weinheim, 1999, p. 553.
[18] K.L. Yeung, E.E. Wolf, Catal. Lett. 12 (1992) 213.
[19] K.L. Yeung, E.E. Wolf, J. Catal. 135 (1992) 13.
[20] K.L. Yeung, E.E. Wolf, J. Vac. Sci. Technol. A 10 (1992) 651.
[21] S. Tsubota, T. Nakamura, K. Tanaka, M. Haruta, Catal. Lett. 56 (1998) 131.
[22] M. Maciejewski, P. Fabrizioli, J.D. Grunwaldt, O.S. Becker, A. Baiker, Phys. Chem. Chem. Phys. 3 (2001) 3846.
[23] M. Haruta, M. Daté, Appl. Catal. A 222 (2001) 427.
[24] M. Haruta, Gold Bull. 37 (2004) 27.
[25] P. Buffat, J.P. Borel, Phys. Rev. A 13 (1976) 2287.
[26] A.J. Maira, K.L. Yeung, C.Y. Lee, P.L. Yue, C.K. Chan, J. Catal. 192 (2000) 185.
[27] A.J. Maira, K.L. Yeung, J. Soria, J.M. Coronado, C. Belver, C.Y. Lee, V. Augugliaro, Appl. Catal. B 29 (2001) 327.
[28] K.L. Yeung, A.J. Maira, J. Stolz, E. Hung, N.K.C. Ho, A.C. Wei, J. Soria, K.J. Chao, P.L. Yue, J. Phys. Chem. B 106 (2002) 4608.
[29] A.J. Maira, J.M. Coronado, V. Augugliaro, K.L. Yeung, J.C. Conesa, J. Soria, J. Catal. 202 (2001) 413.
[30] K.L. Yeung, S.T. Yau, A.J. Maira, J.M. Coronado, J. Soria, P.L. Yue, J. Catal. 219 (2003) 107.
[31] P.P. Lottici, D. Bersani, M. Braghini, A. Montenero, J. Mater. Sci. 28 (1993) 177.
[32] J. Lynch, Physico-Chemical Analysis of Industrial Catalysts: A Practical Guide to Characterization, Editions Technip, Paris, 2003, pp. 8–9.
[33] S.J. Lee, A. Gavriilidis, J. Catal. 206 (2002) 305.
[34] S.J. Lee, A. Gavriilidis, Q.A. Pankhurst, A. Kyek, F.E. Wagner, P.C.L. Wong, K.L. Yeung, J. Catal. 200 (2001) 298.
[35] D.R. Lide, CRC Handbook of Chemistry and Physics, CRC Press LLC, Boca Raton, 2005, pp. 8–20.
[36] A. Fernandez, A. Caballero, A.R. Gonzalez-Elipe, J.M. Herrmann, H. Dexpert, F. Villain, J. Phys. Chem. 99 (1995) 3303.
[37] J.M.C. Soares, P. Morrall, A. Crossley, P. Harris, M. Bowker, J. Catal. 219 (2003) 17.
[38] C. Morterra, J. Chem. Soc. Faraday Trans. 84 (1988) 1617.
[39] M. Primet, P. Pichat, M.V. Mathieu, J. Phys. Chem. 75 (1971) 1216.
[40] K. Tanaka, J.M. White, J. Phys. Chem. 86 (1982) 4708.
[41] P. Konova, A. Naydenov, C. Venkov, D. Mehandjiev, D. Andreeva, T. Tabakova, J. Mol. Catal. A 213 (2004) 235.
[42] F. Boccuzzi, A. Chiorino, J. Phys. Chem. B 104 (2000) 5414.
[43] B. Chang, B.W. Jang, S. Dai, S.H. Overbury, J. Catal. 236 (2005) 392.
[44] G.Y. Popova, T.V. Andrushkevich, Y.A. Chesalov, E.S. Stoyanov, Kinet. Catal. 41 (2000) 805.
[45] J.M. Coronado, S. Kataoka, I. Tejedor-Tejedor, M.A. Anderson, J. Catal. 219 (2003) 219.
[46] A.A. Davidov, in: C.H. Rochester (Ed.), Infrared Spectroscopy of Adsorbed Species on the Surface of Transition Metal Oxides, Wiley, Chichester, 1990, p. 39.
[47] A. Kolmakov, D.W. Goodman, Catal. Lett. 70 (2000) 93.